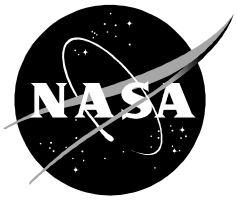
NASA/TM-20240011708



Wind Tunnel Test of a Scale-Model of a Venus Probe to Determine Aeroacoustics Environment

Evan D. Crowe

Metis Technology Solutions

Jayanta Panda, Bruce L. Storms, James C. Ross, Sofia Tafolla, Nathan Eller

NASA Ames Research Center

Anju Gupta, Matthew B Garrison

NASA Goddard Spaceflight Center

December, 2024

NASA STI Program Report Series

The NASA STI Program collects, organizes, provides for archiving, and disseminates NASA's STI. The NASA STI program provides access to the NTRS Registered and its public interface, the NASA Technical Reports Server, thus providing one of the largest collections of aeronautical and space science STI in the world. Results are published in both non-NASA channels and by NASA in the NASA STI Report Series, which includes the following report types:

- TECHNICAL PUBLICATION. Reports of completed research or a major significant phase of research that present the results of NASA Programs and include extensive data or theoretical analysis. Includes compilations of significant scientific and technical data and information deemed to be of continuing reference value. NASA counterpart of peer-reviewed formal professional papers but has less stringent limitations on manuscript length and extent of graphic presentations.

- TECHNICAL MEMORANDUM. Scientific and technical findings that are preliminary or of specialized interest, e.g., quick release reports, working papers, and bibliographies that contain minimal annotation. Does not contain extensive analysis.

- CONTRACTOR REPORT. Scientific and technical findings by NASA-sponsored contractors and grantees.

- CONFERENCE PUBLICATION. Collected papers from scientific and technical conferences, symposia, seminars, or other meetings sponsored or co-sponsored by NASA.

- SPECIAL PUBLICATION. Scientific, technical, or historical information from NASA programs, projects, and missions, often concerned with subjects having substantial public interest.

- TECHNICAL TRANSLATION. English-language translations of foreign scientific and technical material pertinent to NASA's mission.

Specialized services also include organizing and publishing research results, distributing specialized research announcements and feeds, providing information desk and personal search support, and enabling data exchange services.

For more information about the NASA STI program, see the following:

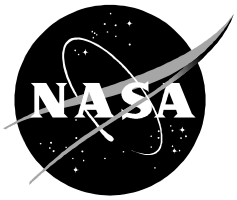
- Access the NASA STI program home page at http://www.sti.nasa.gov

- Help desk contact information:

https://www.sti.nasa.gov/sti-contact-form/

and select the "General" help request type.

NASA/TM-20240011708



Wind Tunnel Test of a Scale-Model of a Venus Probe to Determine Aeroacoustics Environment

Evan D. Crowe

Metis Technology Solutions

Jayanta Panda, Bruce L. Storms, James C. Ross, Sofia Tafolla, Nathan W. Eller

NASA Ames Research Center

Anju Gupta, Matthew B. Garrison

NASA Goddard Spaceflight Center

National Aeronautics and

Space Administration

Ames Research Center

Moffett Field, CA 94035-1000

December 2024

Acknowledgments

Funding provided by the NASA Engineering and Safety Center (NESC) is gratefully acknowledged. The authors would also like to acknowledge the assistance of David Keil in preparing the wind tunnel model and installing the test fixture as well as Miranda Poltorak for her facility support during testing.

Abstract

The Zephyr probe for NASA's DAVINCI project is being designed to fly to Venus and collect measurements to characterize the Venusian atmosphere while it descends towards the surface. Despite a slow descent speed as the probe approaches the surface, the very dense atmosphere means the vibro-acoustic environment that the probe must withstand could be very harsh. A wind tunnel test campaign was conducted to characterize the surface-pressure fluctuations (acoustics) on the external surface of the probe during the descent. The goal was to provide forcing functions for vibro-acoustic analysis of all instruments inside the probe. A 25% scale-model of the Zephyr probe was manufactured, instrumented with 18 microphones, and tested in two wind tunnels located in the Fluid Mechanics Lab at NASA Ames Research Center at velocities ranging from 13 m/s to 48 m/s. Trip strips were added to the model to ensure a turbulent boundary layer on the model. Microphones were located appropriately to provide spectra of pressure fluctuations in regions with different flow characteristics as well as for calculating various two-point statistics. The acoustic spectra measured in the wind tunnel tests were scaled up to flight-scale using the estimated flight trajectory information. Besides fluctuating surface-pressure measurements, hot-film velocity measurements as well as smoke-laser flow visualization were conducted to better understand the flow around the probe. Lastly, several different geometry configurations were tested to see whether any reduction in acoustic levels could be achieved, but none of the configurations that were tested offered significant improvements. The flow visualization showed 3 primary flow regimes on the model: an attached turbulent boundary layer on the front of the model, a region of separated flow upstream of the flared lip, and a large, separated wake at the rear of the model. The acoustic spectra generally show three different shapes corresponding to these flow regions, with the highest levels seen at the rear of the model, and directly in front of the drag plate. The scaled overall levels of pressure fluctuations were found to be high: in the range of 130dB to 155dB.

Table of Contents

Abstract 3
1 Introduction 2
2 Test Set-up and Procedures 4
3 Results 11
4 Summary and conclusions 26
5 References 26

Nomenclature

DAVINCI: Deep Atmosphere Venus Investigation of Noble gases, Chemistry, and Imaging
OASPL: Overall sound pressure level
LS: Lifesaver wind tunnel
PSD: Power spectral density
SLA: Stereolithography
TC2: Test cell 2 [wind tunnel]
VASI: Venus Atmosphere Structure Investigation
VMS: Venus Mass Spectrometer

1 Introduction

The Deep Atmosphere Venus Investigation of Noble gases, Chemistry, and Imaging (DAVINCI) mission aims to provide a better understanding of the Venusian atmosphere. The mission will send a probe (named 'Zephyr') to Venus and collect spectroscopic data, surface imaging, chemical compositions, and other measurements while it descends through the atmosphere [1]. The flow of atmospheric gases over the probe outer surface will create surface-pressure fluctuations, which potentially can excite the structural modes of the outer skin of the probe, and then transmit inside creating the vibro-acoustics environment for various instruments. It is known that the amplitudes of surface-pressure fluctuations (p') is directly proportional to the dynamic pressure ($q = 0.5\rho U^2$, ρ: gas density, U: velocity) of the gas flow over the probe surface. The very high density of the Venusian atmosphere means that the pressure fluctuations on the probe surface during the final phase of the descent will be much higher than on Earth for the same velocity. There is a concern that the resulting vibration levels could be large enough to prevent various instruments inside the probe from functioning. This motivated the present wind tunnel test campaign to measure the surface-pressure fluctuation (acoustic) levels on a scale-model of the probe. The data will be used to create a forcing function for vibro-acoustics analysis of the probe and the instruments within. This report will describe the wind tunnel test and its results.

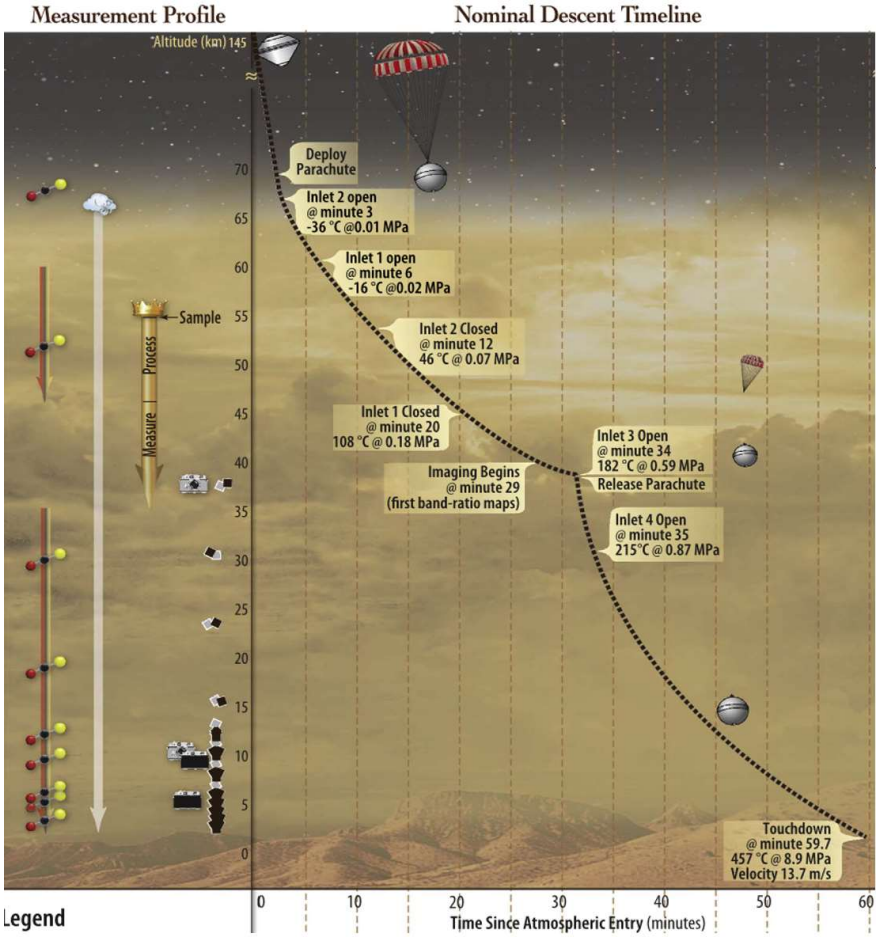


***Figure 1**: Overview of DAVINCI mission trajectory. Insert is depiction of the Zephyr probe [1].*

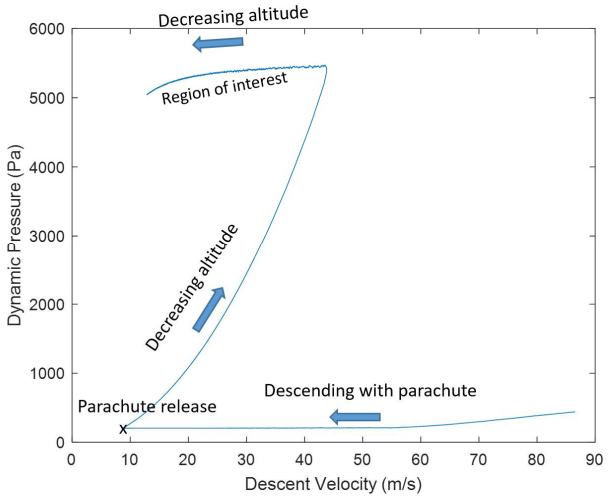


***Figure 2**: Variation of dynamic pressure and velocity during descent of Zephyr probe*

The Zephyr probe first enters the Venusian atmosphere in an aeroshell with a thermal protection system. This shell is then shed and a parachute is deployed. Figure 1 shows an overview of the descent after the aeroshell is shed. At around 70 km altitude a parachute is deployed to slow the velocity of descent. Around an altitude of 38 km the parachute is cut. After a brief acceleration, the thick atmosphere continues to slow down the free-falling probe from a speed of ~44 m/s to 13 m/s at touchdown to the Venus surface.

Figure 2 shows a plot of the velocity versus dynamic pressure during Zephyr probe's descent. The bottom leg of the plot corresponds to the stage when the probe is attached to the parachute. The gas density in this stage of the fall is low; therefore, the dynamic pressure experienced by the probe is also low. As the parachute is cut the probe velocity increases; the probe passes through the thicker part of the atmosphere and the dynamic pressure shows a sharp rise. The topmost part of the plot shows a slowing probe passing through atmosphere whose density is increasing very fast, resulting in a near constant dynamic pressure. Thus, the portion of the descent after the parachute is released (indicated on Figure 2) is the most problematic due to the high dynamic pressure, which prescribed the speed range of interest for the testing. Besides the large dynamic pressure, the Venus atmosphere presents an extreme environment due to its very high atmospheric pressure and temperature.

1.1 Zephyr Probe Geometry

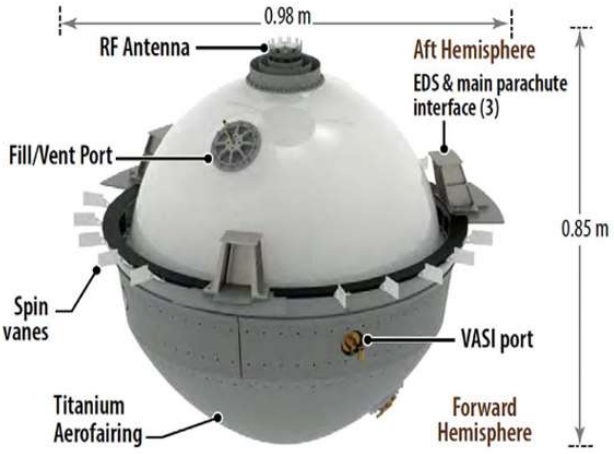


***Figure 3**: Zephyr probe with various components labeled [1].*

The Zephyr probe, shown in Figure 3, is a nearly spherical probe with a flared lip along the thickest part of the probe that fixes the flow separation location. Behind the flanged lip there is a small recess that forms a cavity. It also features drag plates whose size is designed to tune the drag coefficient to achieve the desired trajectory. An array of spin vanes are also included to provide rotational stability during the descent. The outer surface of the probe is a thin fairing that provides a smooth aerodynamic surface and covers the internal structure of the probe. In between the aeroshell and the internal structure is another cavity.

Two instruments protrude from the surface of the aeroshell- the Venus Mass Spectrometer (VMS) and the Venus Atmosphere Structure Investigation (VASI). These protrude through holes in the aeroshell which then exposes the internal cavity to the external flow. In addition to the VMS and VASI probes, there is a window port on the front of the model that forms a wide, shallow cavity. These geometric features of the probe were considered relevant to the acoustic environment during the probes descent towards Venus. Section 2.1 will describe how they were modeled in the wind tunnel model.

1.2 Vibro-acoustic modeling input determination

The primary goal of this test campaign was to create acoustic forcing functions for vibro-acoustics analysis. This is done by first measuring acoustic spectra on a scale-model in the wind tunnel. These spectra are nondimensionalized, then scaled up to the flight-scale using the scale and flight parameters from the full-scale probe descending through the Venus atmosphere.

These flight-scaled spectra are part of the 'joint acceptance function', Φ_{pmn}, which is calculated by the vibro-acoustic analysis software [2] [3]:

$$\Phi_{pmn}(\omega) = \iint_{k_x,\, k_y} S\left(k_x,\, k_y,\, \omega\right) \left|\Phi_{mn}(k_x,\, k_y)\right|^2 dk_x\, dk_y \tag{1}$$

where $\Phi_{mn}(k_x,\, k_y)$ are the spatial mode shapes as a function of x and y wavenumber, respectively. $S\left(k_x,\, k_y,\, \omega\right)$ is the cross-spectrum of pressure fluctuations and is approximated using Corcos model:

$$S(\boldsymbol{x}_1,\, \boldsymbol{x}_2; \omega\,) = G(x_1, \omega) e^{-C_x k_{cx} |\Delta x|}\, e^{-C_y k_{cy} |\Delta y|}\, e^{-i k_{cx} |\Delta x|} \tag{2}$$

Where $G(x_1, \omega)$ is the autospectrum, C_x and C_y are axial and azimuthal decay coefficients, respectively, and k_{cx} and k_{cy} are wavenumbers. The results of this test campaign will define the parameters of Corcos model in Equation 2.

2 Test Set-up and Procedures

2.1 Wind Tunnel Model

The wind tunnel model is a 25% scale-model of the full-size zephyr probe and was printed using a Formlabs 3L SLA printer and the Formlabs 'Rigid 10K' resin. This resin was chosen for its high strength and dimensional accuracy. Figure 4 shows a CAD rendering of the model along with the axes that specify the microphone coordinates. The origin of these axes is located in the center of the model, aligned axially with the rear edge of the flared lip. The majority of geometrical details and protuberances were included in the model, however, manufacturing the cavities exactly as designed would be difficult, so they were modeled in the wind tunnel model as cavities of different shape but similar (scaled) volume. The cavities in the wind tunnel model can be seen in the section view of Figure 5. The model was designed with swappable inserts for various components so that different geometric configurations could be tested.

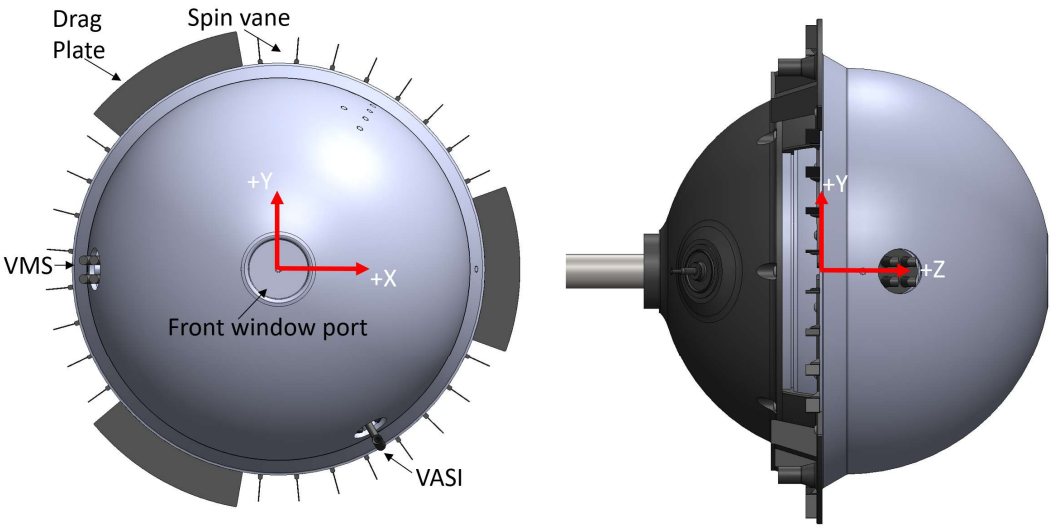


***Figure 4**: CAD rendering of wind tunnel model including coordinate system.*

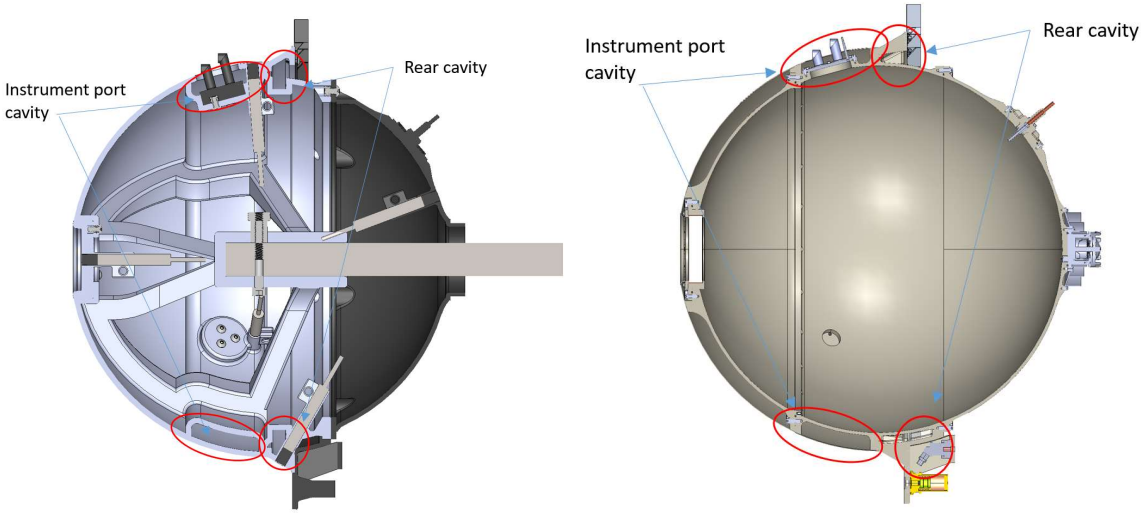


***Figure 5**: Section view of wind tunnel model (left) and Zephyr probe (right)*

***Table 1**: Model configurations and descriptions*

Model Configuration	Description
1: baseline	Baseline case
2: perpendicular wall inst. port	Instrument ports closed with walls perpendicular to the aeroshell
3: tangent wall inst. port	Instrument ports closed with wall flush to the surface of the aeroshell
4: sealed inst. port	VASI and VMS probes completely removed and port capped
5: closed front window	Front window is closed and replaced with a flush surface
6: small drag plates	40 degree sweep drag plates are swapped with 25° sweep drag plates
7: closed rear cavity	Rear cavity behind the rear lip of the aeroshell is filled with a plug
8: 11 degree fin angle	0° spin vanes are replaced with spin vanes with 11° twist

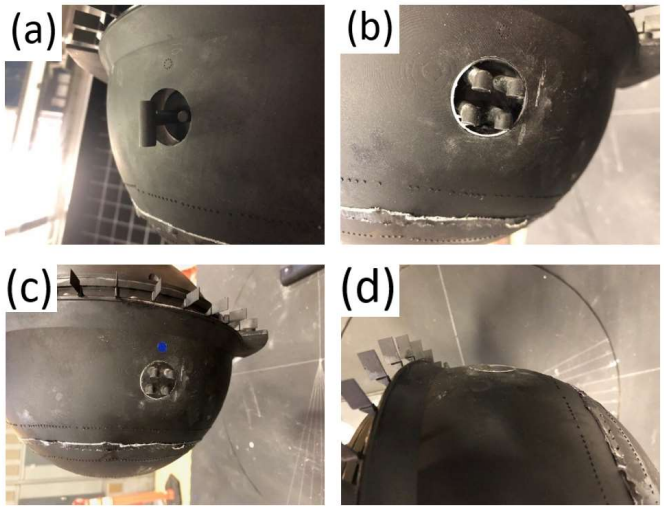


Figure 6*: Instrument port treatments. (a) config. 1: baseline (b) config. 2: perpendicular wall. (c) config 3: tangent wall (d) config. 4: sealed instrument port*

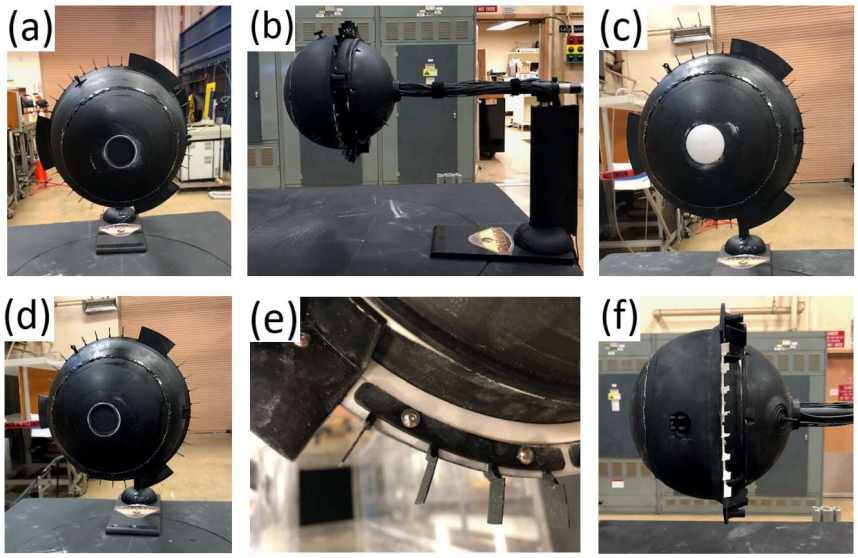


Figure 7*: (a,b) config. 1: baseline. (c) config. 5: filled in front window. (d) config. 6: 25 degree drag plates. (e) config. 7: filled rear cavity (f) config. 8: 11° spin vanes*

One important difference between the present wind tunnel test and the environment during Venusian descent is a difference in the Reynolds number (discussed later in the report). The very high Reynolds number encountered during descent is expected to create a fully turbulent boundary layer on the probe. To ensure the boundary layer on the scale-model was also turbulent, three rows of 0.3mm trip dots were added to the front of the model. These trip dots were deemed to be of insufficient height, so a 1mm tall trip of zigzag tape was also installed on the front of the model. The trip dots and zigzag tape can be seen in photographs of the different model configurations shown later in the report.

Seven different model configurations tested the sensitivity of the acoustic levels to various geometry changes. Some changes focused on probe geometries that were hypothesized to create large pressure fluctuations such as the instrument ports, front window port, and the rear cavity, while others were designed to span the range of certain design parameters that were not yet finalized, like the drag plate size and spin vane angle. Table 1 provides a description of all model configurations, and Figure 6 and Figure 7 show images of the different configurations.

2.1.1 Microphone sensors

Eighteen ¼" diameter, free-field, condenser microphones (G.R.A.S. Type 40BF microphones fit to Type 26AC preamplifiers) were installed inside the model to measure the surface-pressure fluctuations. The cables came out of the rear side of the model and were routed over the model sting and the strut to a bank of power modules and signal conditioners (G.R.A.S. Type 12AG). The outputs of the latter were digitized by 16-bit, simultaneous, analog-to-digital converters at a rate of 20,000 samples/s and stored in a PC. The data resulting from this test campaign is meant to be used in a vibro-acoustic analysis of the probe. In such an analysis, it is typical to divide the vehicle into different zones based on anticipated flow physics or internal structure. The microphones were located to provide data at locations convenient for this analysis. A cluster of microphones were placed in a 'L' shape to allow for calculating cross-correlations between microphone signals- another required data product for the vibro-acoustic analysis. These requirements led to the microphones being placed in a line on the front of the model and the rear, with additional microphones placed behind geometry features that might produce loud noise, namely the drag plate, VMS and VASI probes, front window port, rear cavity, and rear vent port. Figure 8 shows the microphone positions (in model scale) and their numbering scheme, and Table 2 lists the coordinates of their location on the model according to axes defined in Figure 4.

The wind tunnel model included integrated microphone mounts with a perforated screen printed directly into the surface of the model. On the inside of the model, split tube-like features extended down from the surface which fit the quarter-inch microphones, shown in Figure 9.

Table 2: *Microphone location coordinates*

Microphone Number	X (mm)	Y (mm)	Z (mm)
1	29.0	50.2	-73.3
2	34.7	60.0	-64.7
3	21.6	65.9	-64.7
4	39.7	68.8	-54.5
5	-36.8	0.0	-84.1
6	93.1	9.5	-33.4
7	117.5	0.0	7.2
8	51.7	89.5	-4.6
9	-113.3	0.0	22.7
10	56.6	-98.1	23.5
11	56.8	98.3	18.9
12	56.0	97.0	33.1
13	54.2	94.0	48.1
14	51.7	89.5	61.4
15	48.3	83.7	74.0
16	44.0	104.7	18.9
17	38.9	95.8	61.4
18 (open window)	0.0	0.0	121.3
18 (closed window)	0.0	0.0	127.9

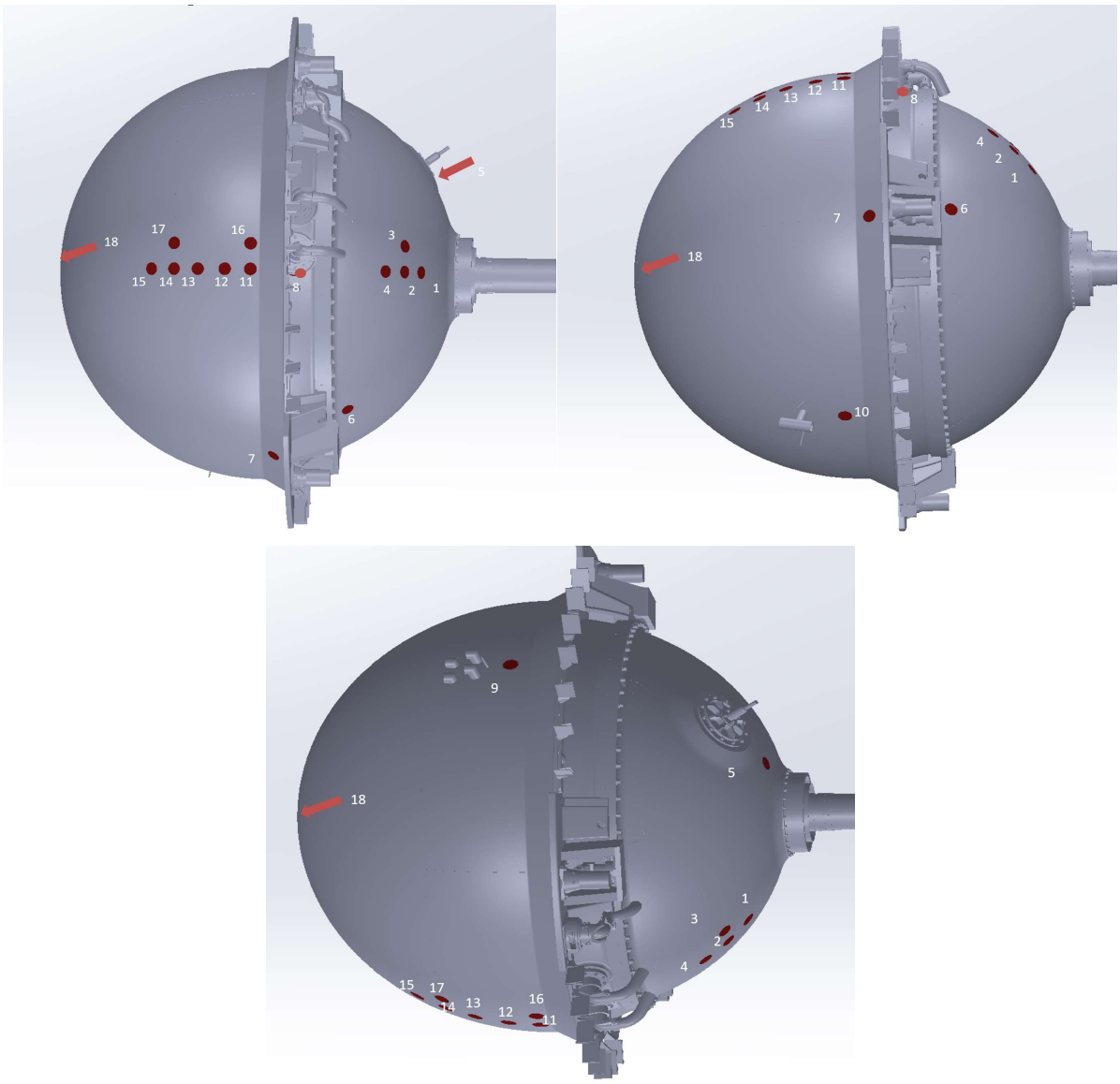


***Figure 8**: Microphone positions and numbering. Different views are different rotations of the model so all microphones can be seen.*

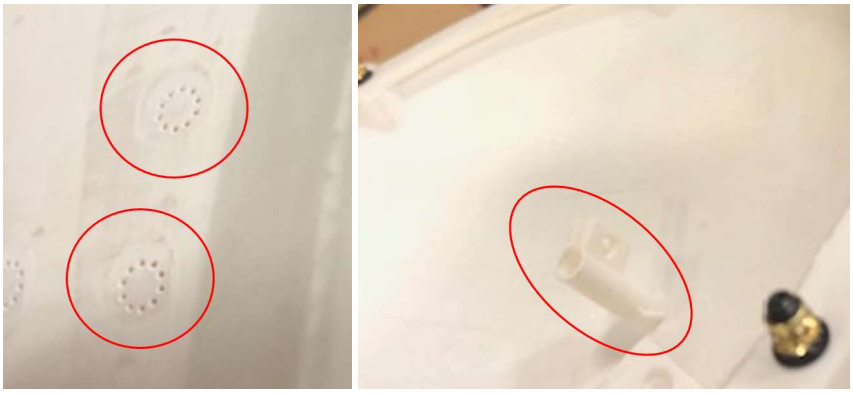


***Figure 9**: Microphone 'screens' (left) and mount (right)*

2.2 Test Plan and Procedure

The test matrix was designed based on the trajectory that the Zephyr probe will experience while it descends in the Venus atmosphere. The trajectory was provided by the aerodynamics team from the DAVINCI project. The probe is expected to encounter a speed range of 13 m/s - 45 m/s and could see variations in angle of attack up to +/- 10 degrees. The Lifesaver wind tunnel has a max velocity of 25 m/s, so data were collected at 5 speeds ranging from 13 m/s - 25 m/s and also at angles of attack of -10°, -5°, 0°, 5°, and 10°. This velocity and angle sweep was completed for three roll angles, 0°, 45°, and 90° degrees. Figure 7(a) shows the model at 0° roll, and the positive rotation is clockwise looking downstream at the model. Varying the roll angles along with the yaw angles provided unique model attitudes. Testing at all yaw and roll angles was completed for only the baseline configuration. The other 7 configurations were tested at 0 degree roll and yaw only, for the entire velocity range.

The first round of testing was completed in the Lifesaver tunnel. After reviewing data, it was decided to continue testing the baseline configuration only in the Test Cell 2 wind tunnel, which is capable of reaching speeds up to 48 m/s. The entire roll and yaw sweep was performed in this wind tunnel for the velocities of 20.0, 25.0, 31.3, 37.6, 44.0, and 48 m/s (tunnel max speed). The last speed exceeds the maximum speed expected during the descent but was included for completeness.

2.3 Wind Tunnel Descriptions

2.3.1 Lifesaver wind tunnel



***Figure 10**: Lifesaver tunnel*

The Lifesaver tunnel at the Fluid Mechanics Laboratory (FML) at NASA Ames Research Center (ARC) is a fan driven in draft tunnel powered by a 15 hp motor. The fan is located upstream of the plenum which contains screens to condition the flow. After the plenum section the flow enters a contraction section followed by an approximately 9.5 foot long constant area section with a 24” x 24” cross section. After this section, the flow exhausts as an open jet over a 30” x 30” platform. It was decided to place the probe in the open jet with the vertical strut mounted on the platform. On this platform is a 20” diameter turn table which provides the ability to yaw the model.

The test setup in the Lifesaver wind tunnel consisted of a vertical support (strut) and a 16” long horizontal sting. The sting mounted to an internal structure inside the model (see Figure 5). The vertical support was fixed to a half inch thick aluminum plate that set back the vertical support from the rear edge of the turn table. The arrangement allowed for extending the sting portion of the mount while still having the model approximately at the center of the turn table. The center of the probe model was approximatley 13” from the beginning of the open jet.

The vertical support was covered in a fairing to minimize the generation of self-noise. The fairing is a McMasters-Henderson airfoil shape with passages for the microphone cables. The McMasters-Henderson airfoil minimized self-noise generation [4]. The microphone cables were fixed to the sting with velcro straps, passed down through the fairing, and then draped off the rear of the test section platform where they plug into their respective amplifiers.

2.3.2 Test Cell 2 wind tunnel



***Figure 11**: TC2 Wind Tunnel test installation*

The Test Cell 2 wind tunnel (TC2) at the Fluid Mechanics Laboratory at NASA ARC features a large inlet and a 48" x 32" test section with a large turntable. It is powered by the FML compressor, which sucks air through the inlet, a plenum, and a contraction section, followed by a test section and a sonic throat. The air-speed is controlled by opening or closing the sonic throat downstream of the test section.

The mounting of the model in the TC2 wind tunnel was nearly identical to that of the Lifesaver setup, except that the vertical support (strut) is taller, 16" vs 12", so that the model is centered in the larger test section. A taller fairing was manufactured to accommodate the larger vertical support. The microphone cables passed through a slot in the turn table down to the microphone amplifiers which were placed beneath the test section.

2.3.3 Empty tunnel background pressure fluctuations

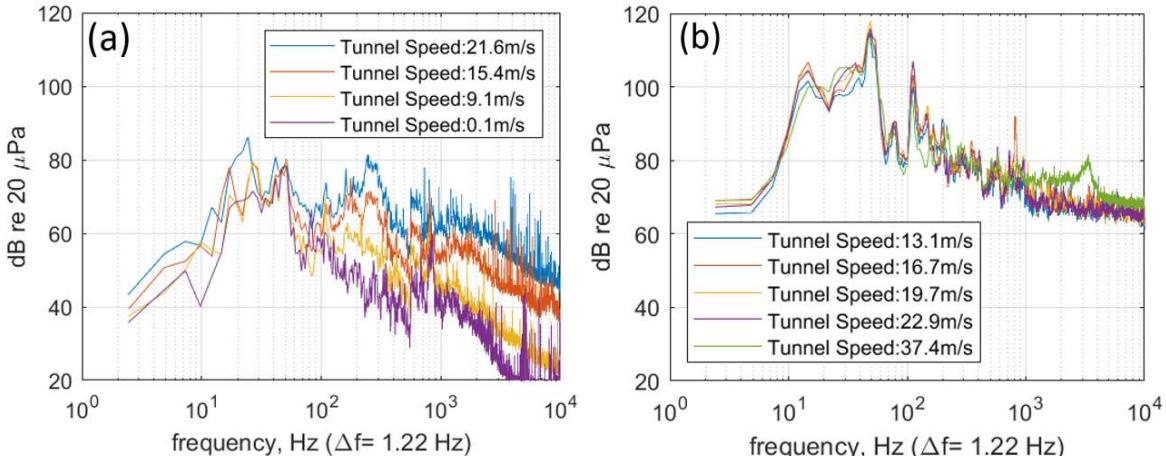


***Figure 12**: Spectra of background pressure fluctuation for (a) Lifesaver tunnel and, (b) Test Cell 2 tunnel at indicated flow speeds.*

Prior to viewing acoustic spectra measured on the wind tunnel model the wind tunnel background spectra must be described so that it may be recognized when the model spectra are contaminated by features of the wind tunnel background noise. These background spectra were measured using ¼" G.R.A.S. Type 40BF condenser microphone fitted with a flow-inducing tone eliminator ("FITE") windscreen and mounted to a 'penguin head' type strut that minimizes microphone self-noise and noise generated by the mounting strut [4]. Figure 12a shows the background spectra for the Lifesaver wind tunnel at a speed range of 9 m/s to 27 m/s. Though the majority of the background spectrum is low enough to not impact the measurements made on the model, the data in some quieter regions of the model are somewhat contaminated by the background noise. In particular, for microphones on the front half, the ~250Hz tone is apparent, as will be described later. Test Cell 2 background spectra exceed 100dB at several frequency ranges. The large noise levels at and below 100Hz are especially problematic since the spectra generated by the probe model is expected to have a large low-frequency content. This motivated the choice to use as much of data collected from the Lifesaver tunnel as possible. TC2 data was used to cover the higher speed part of the trajectory. An advantage of the TC2 data was that the background noise peaks did not change with velocity. This made them easily identifiable in the spectra collected from the Zephyr model.

3 Results

3.1 Flow Visualization

To gain insight of the flow features that drive the acoustic fluctuations, flow visualization was performed using a laser light sheet and injecting smoke into the flow from the front of the model. To accomplish this, a 10mW laser was spread into a sheet using a pair of cylindrical lenses. Because of the class 3B category of the laser, a containment box had to be constructed to contain the laser hazard. This box was mounted atop the Lifesaver tunnel and the laser sheet propagated downward over the model, as shown in Figure 13. Smoke was injected out the front of the model using a special inlet with a 'showerhead' type outlet that ensured the smoke was distributed evenly. Most images were taken at a low speed, about 4.5 m/s. Some images were taken at higher speeds, and the primary flow features are similar although the image quality was often not as good due to the smoke dispersing more quickly.

The flow visualization highlighted the large wake behind the model, shown in Figure 14. In this wake there is large-scale recirculation which can be observed in videos taken during testing. Smoke was injected into the wake behind the model using a long smoke wand and was observed to flow upstream along the surface of the model and up towards the edge of the wake. This also drove a smaller counter-rotating recirculation region directly behind the flared lip.

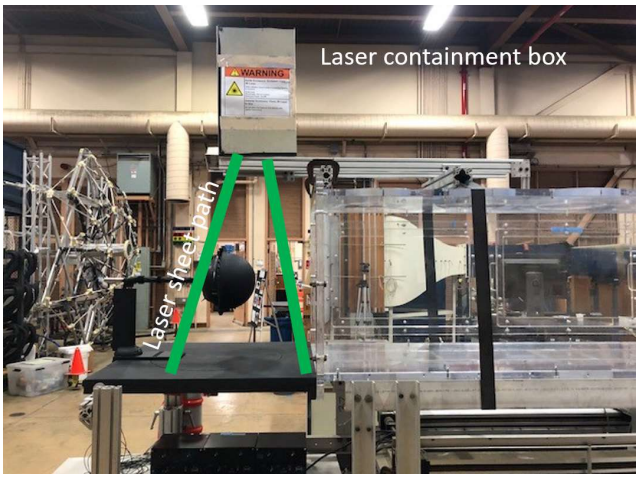


***Figure 13**: Flow visualization setup*

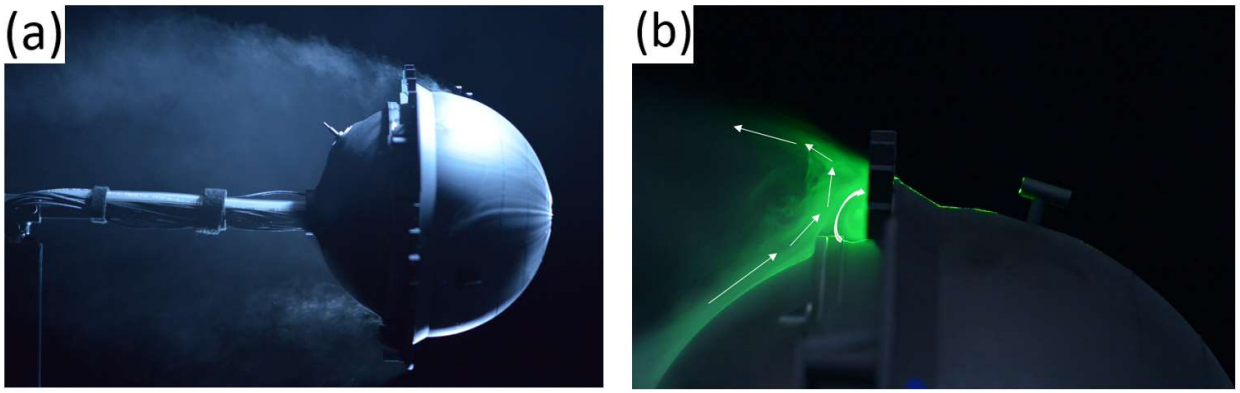


Figure 14*: Smoke visualization showing (a) large wake behind the model and (b) recirculation zone behind the drag plate.*

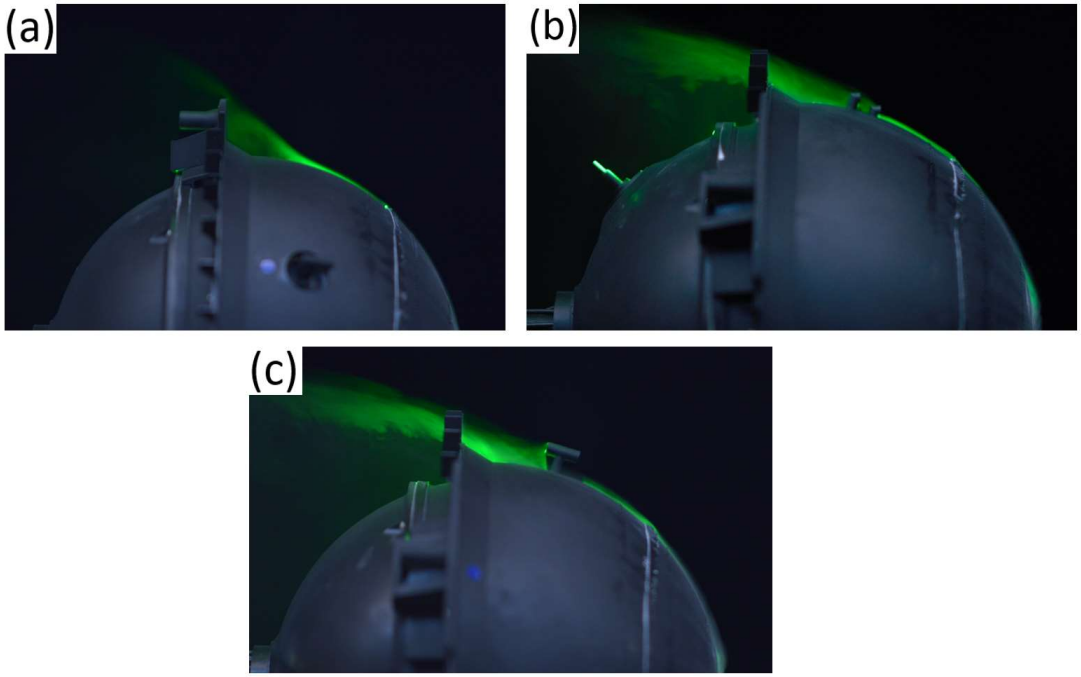


Figure 15*: Flow visualization around various features. (a) Recirculation zone in front of drag plate. U= 13.7 m/s, (b) VMS probe, U= 4.5 m/s, (c) VASI probe, U= 4.5 m/s.*

Other flow visualization testing focused on the drag plate, VASI probe, and VMS probe. Figure 15 shows the flow visualization images for these three features. In front of the drag plate, another recirculation region was observed where the trapped smoke rotated counterclockwise. As the flow separated upstream of the drag plate, it drove this vortex in front of the drag plate. This separated, recirculating zone was found to create large acoustic levels in front of the drag plate.

The VMS and VASI probes were seen to introduce local flow disturbances and there were small wakes behind each probe. Flow visualization images were also collected for the 'capped' probe insert case, where the cavity beneath each probe was capped with a wall tangent to the surface. This did not cause an appreciable change in the wake behind the probes, except making them perhaps slightly smaller.

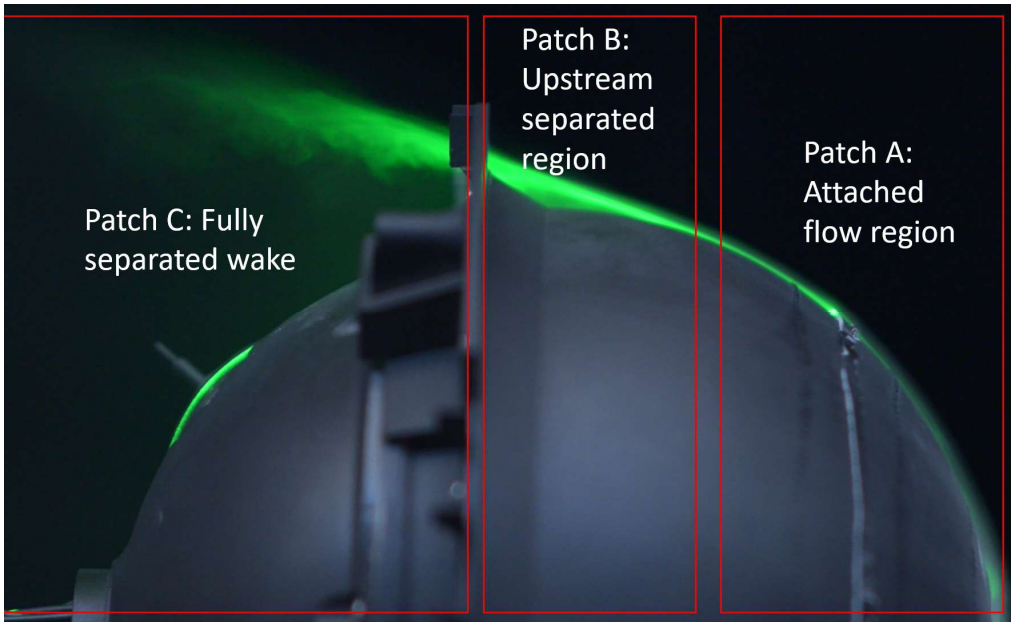


***Figure 16**: Selection of the acoustic zones based on different flow features on the wind tunnel model.*

The flow visualization helped to identify the three regions with similar flow features over the probe (Figure 16). At the front of the probe, the flow remained attached as a turbulent boundary layer (ensured by means of a thick boundary layer trip near the front of the model). The flow over the rear half of the model was an entirely separated wake, with a large amount of recirculation. In the middle of the model, there was a small, separated region upstream of the flared flange and drag plates.

3.2 Baseline Results Overview

3.2.1 Test Cell 2 Background Tone Removal

The data from Test Cell 2 was affected by large amplitude background pressure fluctuations discussed earlier. An attempt was made to remove these background tones from the spectra by cropping out the known tones and replacing them with smooth curves. Other parts of the spectra were unchanged. Some microphones that did not experience very high levels (exceeding the background levels of Figure 12) were heavily affected, while others like those on the rear of the model were less affected and/or not affected at all at higher velocities. Figure 17 shows a spectrum before and after tone removal. Besides aiding interpretation of the spectral data, this process is particularly important for determining maximax spectra which are one of the final data products from this test campaign. All spectra calculated using TC2 data and presented in this report were tone-corrected. Note that the tone removal was applied to model-scale level, before scaling up to the full-scale flight condition.

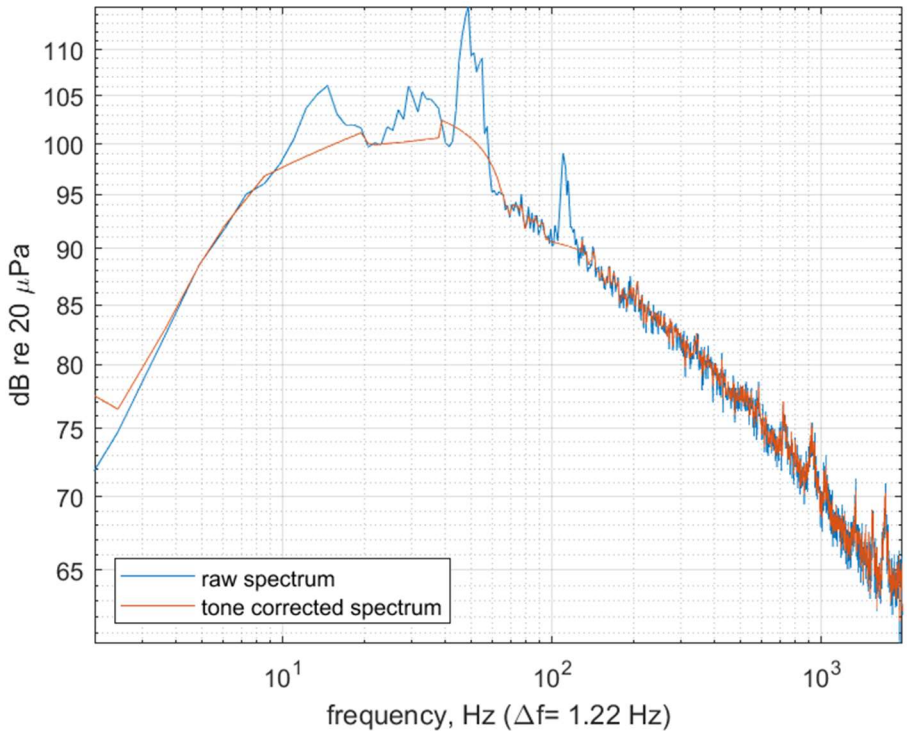


***Figure 17**: Pressure flucutation spectrum (model scale) before and after tone removal, mic 1*

3.2.2 Baseline Pressure Fluctuation Spectra

The pressure fluctuation spectra from the individual regions of Figure 16 were similar in shape. Figure 18 shows representative acoustic spectra from each region. Data over the entire velocity range measured is shown. Data were collected at 20 and 25 m/s in the TC2 wind tunnel for comparison to the Lifesaver tests and was found to agree well (not shown). No data are shown for different yaw and roll angles, since the spectra shapes and amplitudes were very similar (within 1-2dB).

Figure 18(a) shows spectra measured by microphone 3, and are representative of the large region of separated flow on the rear half of the model. Besides the area in front of the drag plate (this will be discussed in the next section), this region had the highest levels of fluctuations which increased with velocity. A broad peak is present centered on a frequency of ~15 Hz and does not appear to change significantly with velocity. Figure 18(b) shows the spectra from microphone 11, which is located in the small, separated region upstream of the flange. The spectra from microphone 11 have a more complicated shape with one low frequency peak (whose frequency does change with velocity) and higher frequency bump as well. The levels are lower than microphone 3 by several dB at each velocity. The spectra measured in TC2 also show some background tones associated with that tunnel which were removed by the previously described tone removal process. Some artifacts from this processing are visible in the spectra. Figure 18(c) shows microphone 17 which is located near the front of the model where the flow is attached. The spectra in this region have a similar shape to that of microphone 11, but at lower amplitudes and don't feature the higher frequency hump. They do exhibit the ~250 Hz background tone from the lifesaver tunnel which can be observed in all the Lifesaver data, but not the TC2 data.

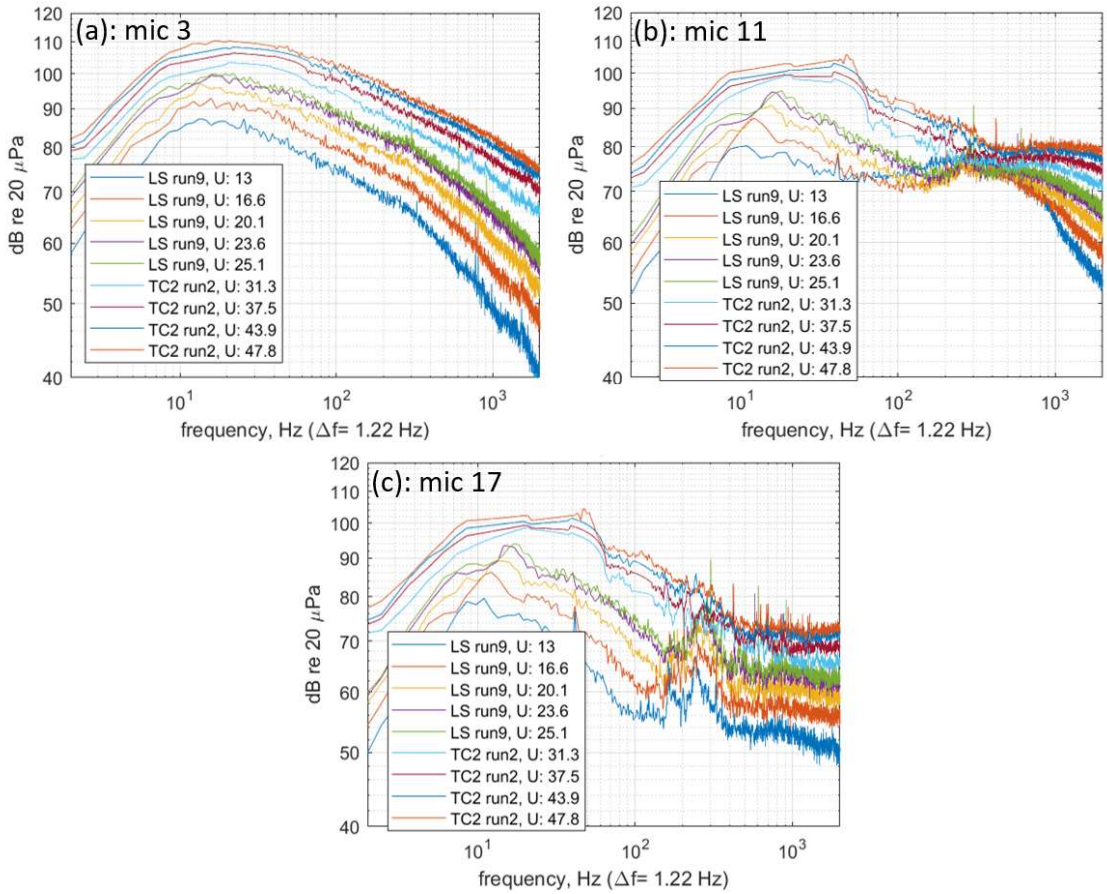


***Figure 18**: Model scale spectra from indicated microphones and at velocities (in m/s) mentioned in the legend. LS: Lifesaver tunnel, TC2: TC2 tunnel.*

3.3 Comparison of different configurations

Figure 19 shows the comparisons between the baseline spectrum and various geometric configurations. After conducting these tests, it was found that the different configurations did not reduce the levels significantly and so no further testing was conducted at different yaw or roll angles.

3.3.1 Probe port treatments

The comparisons of different port treatments are shown in Figure 19(a) and (b) for the max velocity tested, U=25 m/s. The ports in the baseline configuration were open to an internal cavity within the model and it was debated whether this opening and cavity could create a loud tone or otherwise increase levels. Two treatments were tested to close the cavity, one that closed the cavity tangent to the surface (Figure 7(c)), and another that closed it perpendicularly to the outer surface (Figure 7(b)). The last configuration tested had both the VASI and VMS probes removed entirely and replaced with a flush surface (Figure 7(d)).

For both the VMS and VASI probe, the levels measured directly behind the ports were lower than other areas of the model such as the rear half of the model and in front of the drag plate. Additionally, neither of the different treatment options had a significant effect. For the VMS probe, both treatments had similar spectra below ~600Hz, while above this frequency, the levels are a few dB lower for the tangent wall cap (although the baseline level is only 85dB or lower in that part of the spectrum.) However, for the VASI probe, while the perpendicular wall cap again had little effect, the tangent wall cap increased levels below ~800 Hz by several dB. For both instrument ports, removing the instrument entirely significantly decreased the acoustic levels.

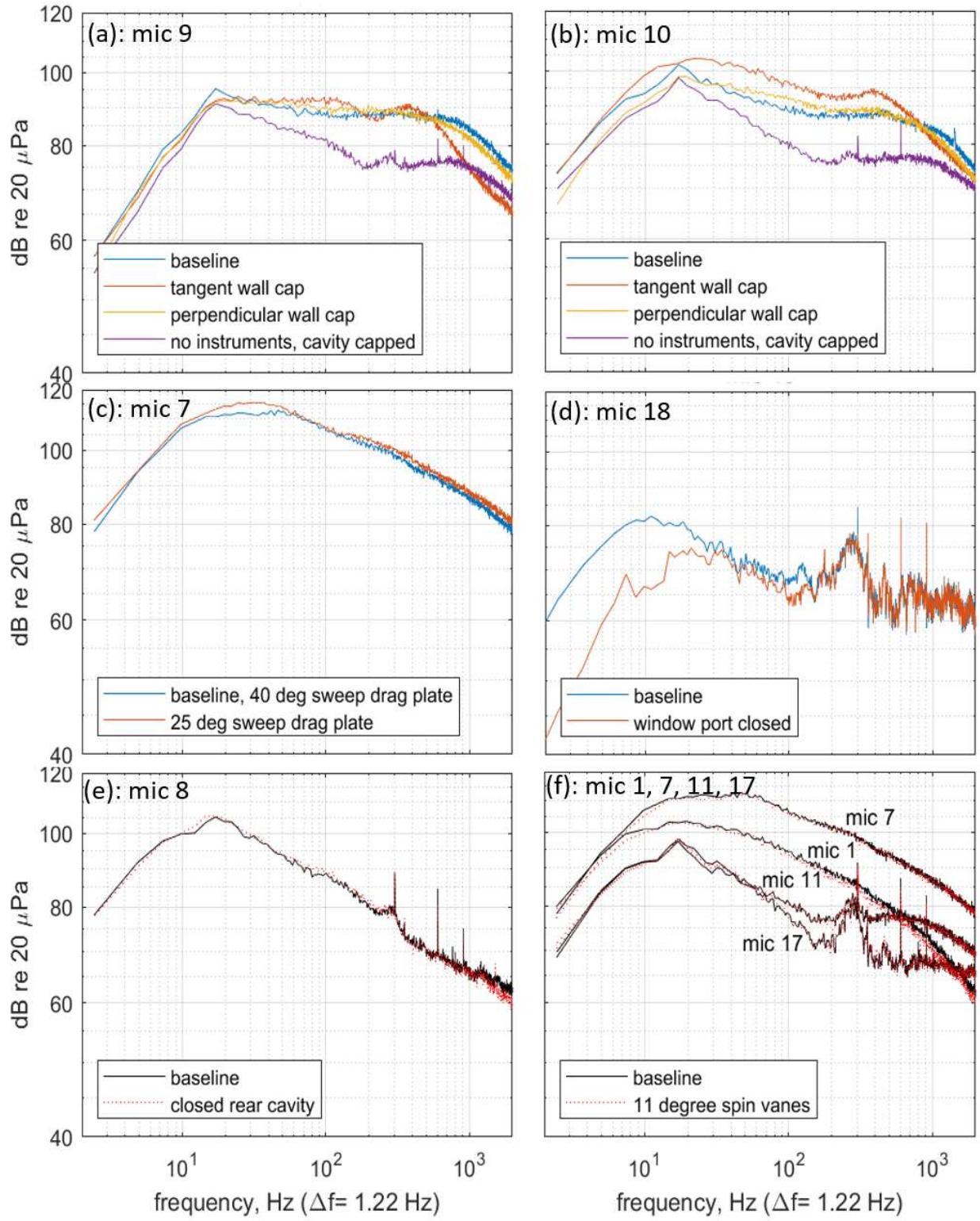


***Figure 19**: Effects of different geometric configurations as indicated in the legend on model-scale spectra. All are shown for U=25 m/s. (a) VMS port: effect of different cavity treatments; (b) VASI port: effect of different cavity treatments; (c) large, 40° vs small, 25° drag plate; (d) Effect of closing front window port; (e) Effect of closing rear cavity; (f) comparison of spectra from various microphones for 0° (baseline) and 11° spin vanes.*

3.3.2 Drag Plate Size

The drag plate size was also varied. The DAVINCI program suggested that 25-40 degrees sweep is roughly the upper and lower bounds of the size of the drag plates and so two sizes were chosen to cover the maximum and minimum size. The larger size (40° sweep) was used for the baseline configuration. Figure 19(c) shows the comparison at U=25 m/s between the larger and smaller drag plate sizes. The smaller drag plate had little effect on the overall spectrum, while slightly increasing levels in a narrow portion of the spectrum between 10-40 Hz.

The probe surface in front of the drag plate experienced the highest pressure fluctuations, perhaps driven by the vortex that forms directly in front of the drag plate seen in Figure 15(a).

3.3.3 Front Window Port

The small recess at the front of the probe was thought to possibly contribute to higher acoustic levels, so a configuration change tested involved replacing the front cap with a rounded cap. For both cases, a microphone was located at the front of the probe. Figure 19(d) shows the spectra from both cases which exhibited very few differences. Though closing the front window appears to reduce levels below 30Hz, this reduction is possibly due to a damaged microphone, since the same reduction was observed after the baseline window port was reinstalled. One part of the spectrum that may be affected is a small peak around 100 Hz in the baseline configuration which goes away when the front window port is closed. Other microphones downstream of the window port were also relatively unaffected by the change in the window port.

3.3.4 Rear cavity

Directly behind the flared lip is the 'rear cavity' shown in Figure 5. Figure 19(e) shows this comparison between the baseline and the configuration where this cavity was filled for microphone 8, located directly behind this cavity. The flow in the region behind the flange is dominated by large scale separation, and microphone 8 exhibits a similar spectra to the other microphones in this region. No clear tone is seen in the baseline because of the rear cavity. Closing the rear cavity has very little effect on the levels measured by microphone 8, as well as other microphones elsewhere on the model.

3.3.5 Spin Vane angle

For the final configuration change, the baseline spin vanes which had a 0° twist angle relative to the free stream flow direction were replaced with spin vanes that had an 11° twist angle. Figure 19(f) shows a selection of microphones representative of all three regions of the model. The spin vanes had a very minimal effect on most microphones. Only the rear half of the probe is affected, and this effect is a very slight decrease at higher frequencies and only can be observed in spectra measured on the rear of the model, such as the microphone 1 spectrum.

3.4 Non-dimensional spectra and flight scaling

These acoustic spectra are meant to be a forcing function input for the vibro-acoustic analysis of the Zephyr probe. Therefore, the spectra measured in the previous section had to be scaled up to apply to the full-scale vehicle plunging through the Venus atmosphere. The two scaling laws assumed for this analysis were the constancy of the pressure coefficient, C_p and Strouhal number, *St,* for Venus flight conditions and the earthly wind tunnel tests (WTT):

$$C_p = \frac{p_{Venus}}{q_{Venus}} = \frac{p_{WTT}}{q_{WTT}} \tag{3}$$

where *p* is the fluctuating pressure, and *q* is the dynamic pressure. The second scaling law, Strouhal scaling, is the following:

$$St = \left(\frac{fD}{U}\right)_{Venus} = \left(\frac{fD}{U}\right)_{WTT} \tag{4}$$

***Table 3**: Flow parameter comparison between wind tunnel and Venus flight conditions*

Parameters	Venus	Air Wind Tunnel Test
Composition	CO2, some H2SO4, Supercritical CO2	N2, O2
Velocity	42.6 m/s – 12.9 m/s	42.6 m/s – 12.9 m/s
Temperature	180 °C – 460 °C	20 °C
Pressure	6X – 90X Earth Atmosphere	Earth Atmosphere
Density	6.06 kg/m3 – 60.6 kg/m3	1.19 kg/m^3
Dynamic pressure	5500 Pa – 5045 Pa	100 Pa-1100 Pa
Reynolds number	10e6 – 24e6	0.3e6-1e6
Sound speed	321 m/s – 413 m/s	340 m/s

where *f* is the frequency, *D* is the probe diameter, and *U* is the free stream velocity. Table 3 shows various relevant parameters to this scaling between wind tunnel tests and Venus flight conditions.

There are several open questions that could affect the accuracy of the scaling laws in this case. The first is in the supercritical CO_2 that makes up part of the Venus atmosphere. The authors know of no measurements of pressure fluctuations underneath a boundary layer from a supercritical CO_2 environment. However, since the same scaling laws are applied both in liquids and gases, it is fair to assume that they will be applicable for a supercritical fluid. The second is the vast difference of Reynolds number between the two cases. The full-scale vehicle will have a Reynolds number up to 24 times the max Reynolds number in the wind tunnel test. It was considered that if the flow is similar (i.e., if a turbulent boundary layer set up on both bodies) the associated acoustics would also be similar. This was accomplished by applying the trip strip at the front of the model. Lastly is the difference in speed of sound, which is relevant to some parameters that are input for the vibro-acoustic analysis.

The nondimensional spectra are calculated from the power spectral density (PSD), prior to converting to third-octave spectra. Nondimensionalizing the power spectral density, which has units of Pa^2/Hz is accomplished by multiplying the PSD by $\frac{U}{Dq}$. After also converting the x-axis to nondimensional frequency, the resulting plot has the quantity $\frac{C_p^2}{\Delta St}$ on the y-axis and *St* on the x-axis. The ΔSt is representative of the fact that each frequency bin has a fixed width.

Plotting the spectra in this way, the spectra should all collapse into a single line if the flow features are self-similar. The nondimensional spectra for microphones 3, 7, and 11 are shown in Figure 20. An interesting behavior can be observed- for microphones on the rear of the model, such as microphone 3, the peak frequency does not follow Strouhal scaling while higher frequencies do. The peak frequencies not following the scaling laws motivated the decisions to conduct additional testing at higher velocities in the TC2 wind tunnel.

Other spectra follow the scaling laws more closely. In particular, spectra from microphone 7 just in front of the drag plate nearly collapses to a single line except for the lowest frequencies. Meanwhile, the microphones on the forward half of the model have a peak frequency that scales according to the Strouhal number even though the levels do not scale well with C_p. The high frequency hump also collapses well except for the lowest two velocities. Figure 20(c) shows this behavior for microphone 11 where the peak frequencies occur around St=0.2 – typical of bluff body shedding. Note that the tone removal distorts the shape of the peak for some spectra measured in TC2.

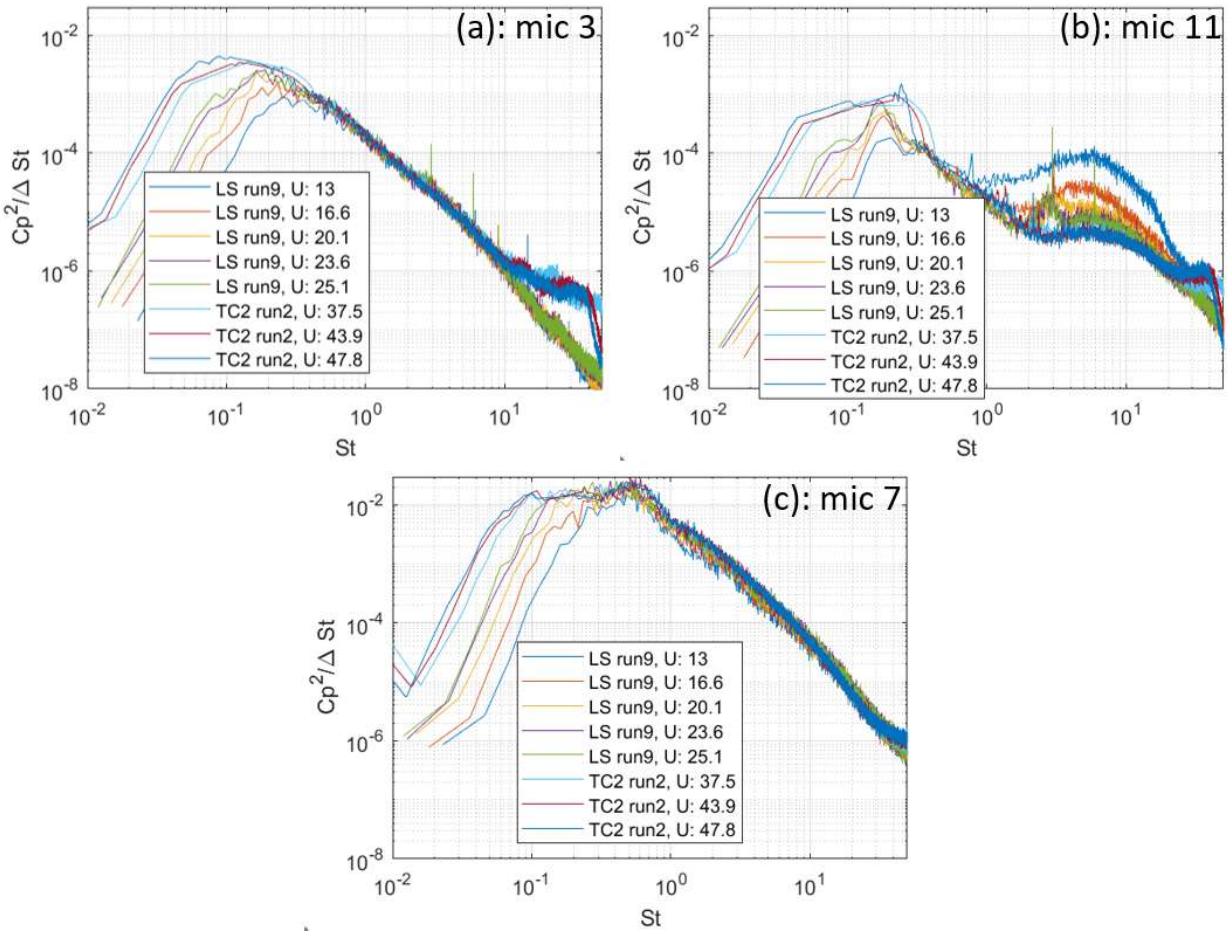


***Figure 20**: Nondimensional pressure fluctuation spectra for indicated microphones and at velocities (in m/s) shown in the legend.*

From the nondimensional spectra the flight-scaled spectra were calculated for each microphone at each velocity. For most cases, scaling up the spectra to flight-scale equated to adding ~30+ dB depending on the velocity. The narrowband flight-scaled spectra were then converted into 1/3rd octave spectra by grouping the narrow band values into 1/3rd octave bands, taking the average value across the 1/3rd octave band, and then multiplying by the bandwidth of the 1/3rd octave band [5]. The flight-scaled spectra are shown in Figure 21.

The Overall Sound Pressure Level (OASPL) is a single value that gives an overall measure of noise measured by a microphone, and is equal to the root mean square value of fluctuating pressure converted to decibels. To provide a complete summary of the microphone data, the OASPL for all microphones is shown in flight-scale in Table 4. It must be noted that the OASPL from the TC2 data were calculated using the tone corrected spectra which affects the OASPL, especially for the microphones on the front half of the model (microphones 11-18). Table 5 shows a similar summary in flight-scale for all geometry configurations tested. Like the spectra, the OASPL of different geometry configurations show that none of the configurations tested offer a significant reduction in sound levels.

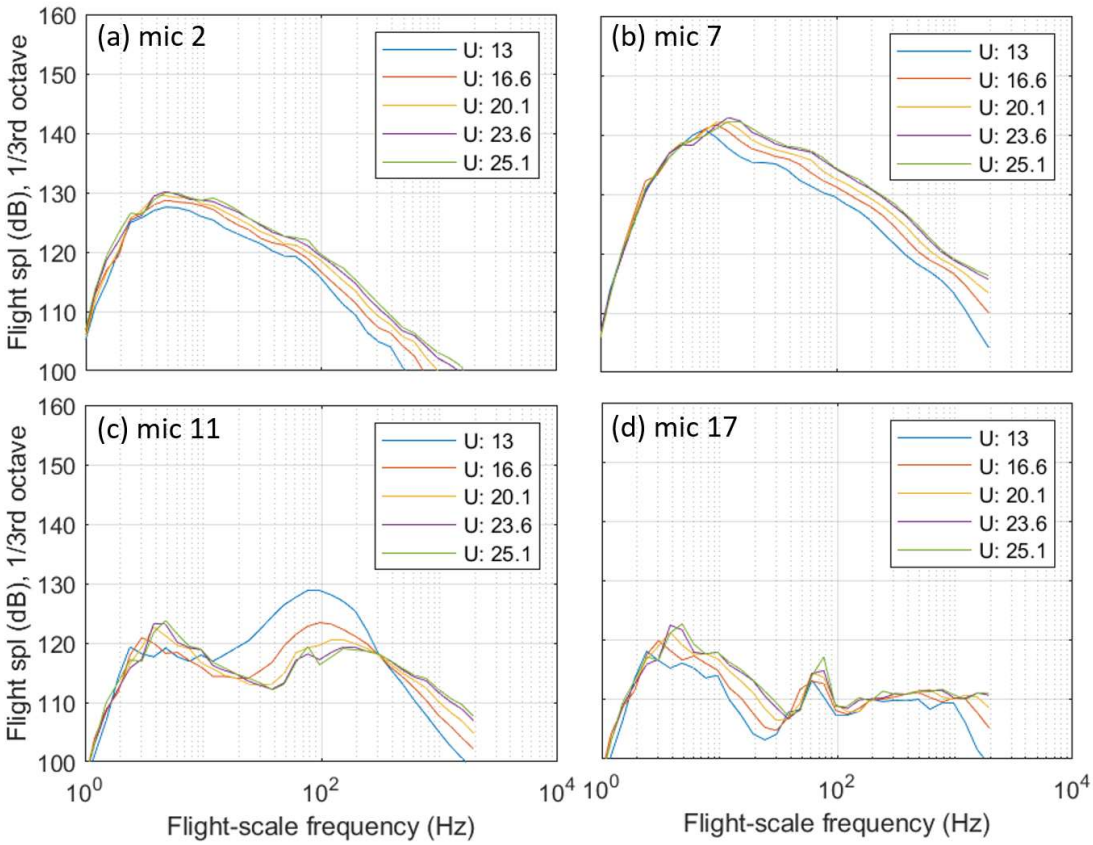


***Figure 21**: Flight-scaled 1/3rd octave spectra from indicated microphones at velocities mentioned in the legend.*

***Table 4**: Overall Sound Pressure Level in dB for all microphones in flight-scale*

Microphone\U (m/s)	13	16.6	20.1	23.6	25.1	31.3	37.5	43.9
1	138.0	139.2	139.7	140.3	140.4	140.8	140.3	138.0
2	136.9	138.1	138.9	139.4	139.6	140.3	139.7	136.9
3	136.4	137.6	138.4	138.8	139.1	140.0	139.3	136.4
4	135.9	137.4	138.3	138.9	138.9	139.9	139.1	135.9
5	141.2	142.2	143.3	143.4	143.5	144.0	143.6	141.2
6	135.0	136.5	137.4	138.1	138.4	139.5	138.6	135.0
7	148.8	150.0	150.9	151.5	151.5	150.9	150.9	148.8
8	133.5	135.3	136.8	137.7	137.9	138.2	137.3	133.5
9	136.7	137.0	137.2	137.6	137.8	139.8	139.4	136.7
10	136.8	137.3	137.9	138.5	138.6	139.9	139.3	136.8
11	137.5	133.3	132.3	132.2	132.3	137.1	134.8	137.5
12	132.2	130.1	130.7	131.1	131.4	136.1	133.9	132.2
13	126.6	127.9	129.2	129.9	130.3	136.0	133.6	126.6
14	125.3	126.7	127.9	128.6	129.0	135.6	133.0	125.3
15	128.0	127.8	128.3	128.5	128.9	135.5	132.6	128.0
16	135.5	131.9	131.5	131.6	131.6	136.1	133.8	135.5
17	126.5	127.9	128.9	129.6	129.9	136.0	133.4	126.5
18	121.7	122.6	123.2	123.7	124.0	135.0	131.8	121.7

***Table 5**: Summary of OASPL for all configurations tested. OASPL is shown for U=25 m/s. For the 11° spin vane configuration, only microphone 1 is shown which showed the greatest difference from the baseline*

Feature	Configuration	Microphone	OASPL (dB)
Front Window	Baseline	18	124.0
	Closed		121.8
VMS	Baseline	9	137.8
	Tangent wall cap		137.2
	Perpendicular wall cap		137.5
	No instruments, cavity capped		129.3
VASI	Baseline	10	138.6
	Tangent wall cap		143.2
	Perpendicular wall cap		138.7
	No instruments, cavity capped		131.9
Rear Cavity	Baseline	8	137.9
	Closed rear cavity		137.6
Drag Plate	Baseline (40° sweep)	7	151.5
	25° sweep		151.1
Spin Vanes	Baseline (0°)	1	140.4
	11° twist angle		140.1

3.5 Determination of Corcos model parameters: convection velocity and decay coefficient

Convection velocity is determined by calculating the cross-spectra between a pair of microphones separated axially by Δx. The gradient of the phase spectra $\frac{d\Phi}{dx}$ along with the axial separation distance Δx provides a measure of convection velocity of the pressure fluctuations:

$$U_c = \frac{2\pi\Delta x}{\frac{d\Phi}{dx}} \tag{4}$$

Figure 22 shows the phase spectra and coherence spectra calculated for the fully separated region of the model ('patch C' in Figure 16). Clearly, the phase spectra are not linear, and the coherence spectrum does not follow any sort of exponential decay fit, as assumed in the Corcos model. However, the phase spectra appear to have two separate frequency regions that are approximately linear. To proceed with the analysis, phase spectra were separated into two different frequency bands by filtering the microphone signals. Then, convection velocities were calculated for each frequency band. This procedure was done for sensors in all three zones.

The phase spectra for the filtered data from patch C are shown in Figure 23. There appears to be two primary regimes- the first is a hydrodynamic wave that convects at 10.8 m/s in the upstream direction, or about 43% of the free-stream velocity and in the opposite direction. The second regime is a wave that convects at a much higher speed in the downstream direction: around 247.8 m/s, which is close to the speed of sound. The difference may be due to small error in determining the axial location of the sensor centers. The coherence spectra are also shown in Figure 24. The low-frequency region follows the decay fit much better than before. However the higher-frequency region, though also improved, is not a very good fit. This is thought to be a limitation of Corcos model, which is developed for attached turbulent boundary layers and does not provide a good fit for the present separated flow situation.

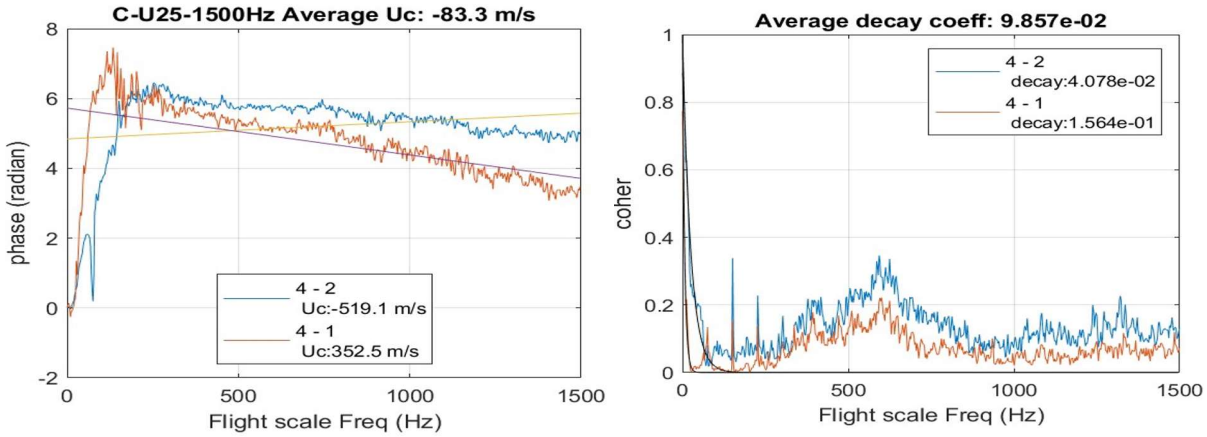


***Figure 22**: phase spectra (left) and coherence spectra (right) between microphone pairs 4-2 and 4-1.*

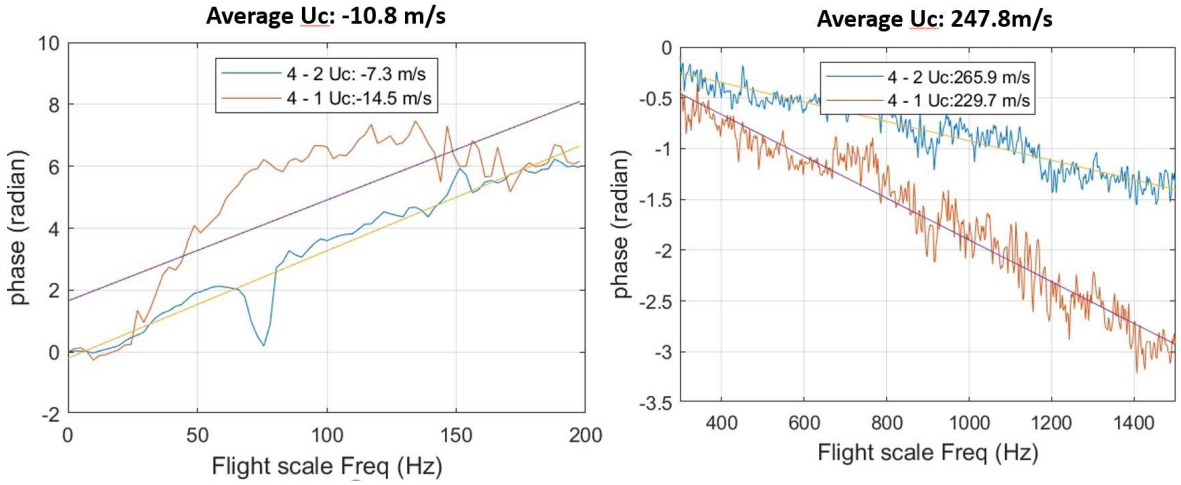


***Figure 23**: Patch C phase spectra for 0-200 Hz low pass filtered data (left) and 300-1500 Hz band pass filtered data (right), for tunnel velocity of 25 m/s, for same microphone pairs as Figure 22.*

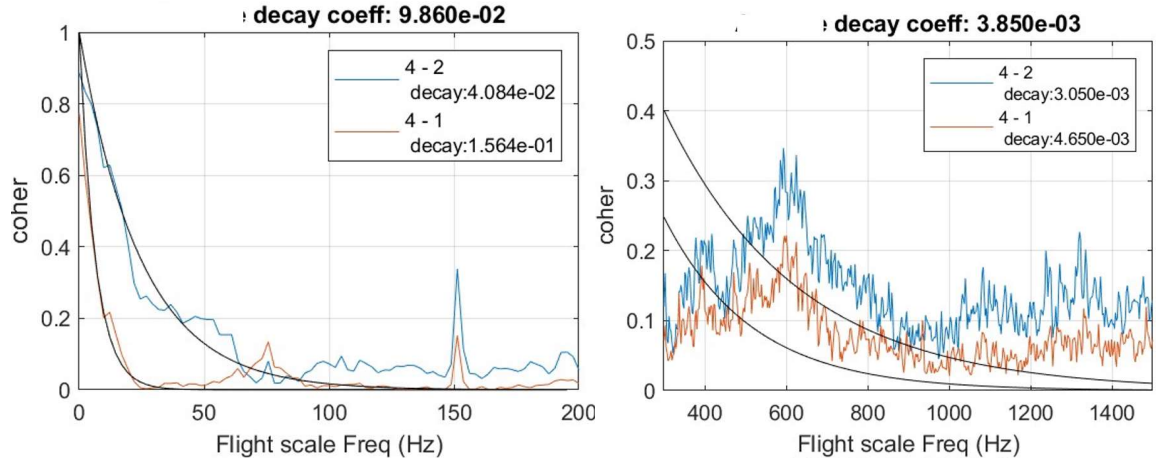


***Figure 24**: Patch C coherence spectra for for 0-200 Hz low pass filtered data (left) and 300-1500 Hz band pass filtered data (right), for tunnel velocity of 25 m/s, for same microphone pairs as Figure 22.*

3.6 Velocity Survey

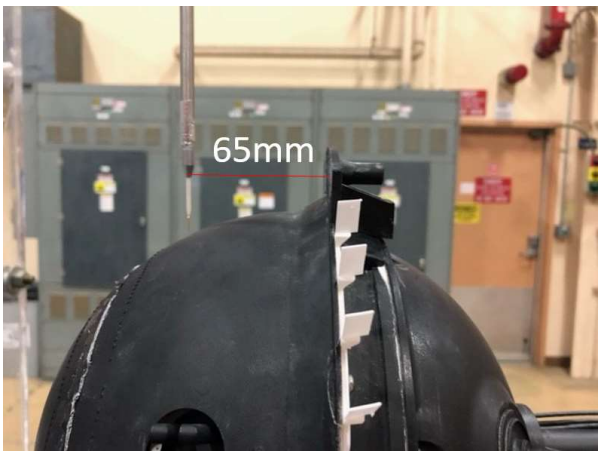


***Figure 25**: Location of hot film probe measurement.*

Velocity surveys at a limited few locations on the model were conducted using a single-wire hot-film probe. A frame was built using extruded aluminum 80-20 based elements to mount a computerized traversing unit which held a Dantec 55R01 fiber-film probe. Traverses in the vertical direction began approximately 1mm from the surface of the probe, and were completed in 4 locations- in front of the VASI and VMS probes, the drag plate, and a location without any feature. All traverses were done at the same streamwise position, and the model was rotated so that the desired feature was located behind the probe. The X,Y coordinates of the survey starting positions based on the model scale coordinate system defined in Figure 4 are listed in the legend of Figure 26 and Figure 27. Note that uppercase X,Y,Z refers to the model coordinate system, while lower case y is used in this section to describe vertical distance from the probe surface.

Figure 25 shows the position of the hotwire at the start of the traverse. The hot film probe was positioned 65mm from the rear surface of the flared lip as shown in Figure 25 (Z = 65 mm) and was then traversed vertically upwards to measure the velocity profile away from the model. The model was rotated to place different features behind the probe, the drag plate, the VMS probe, the VASI probe, as well as a location where none of these features are present.

The hot-film probe was calibrated by placing it in an empty tunnel and recording the voltage output of the probe and the tunnel velocity simultaneously. The tunnel velocity was calculated from static pressure measurements in the tunnels plenum and the test section. The velocity calculation itself is calibrated using a vane anemometer that measured the velocity directly. A 4th order polynomial fit was created using the hot film calibration data and used to calculate the velocity. The temperature was recorded during the calibration and each subsequent survey so that the following temperature correction could be applied [6]:

$$V_{w,r} = V_w \left(\frac{T_w - T_r}{T_w - T_a} \right)^{0.5} \tag{5}$$

Where T_w is the hot film temperature, T_r is the flow temperature during calibration, T_a is the flow temperature during a test, V_w is the probe output voltage, and $V_{w,r}$ is the temperature corrected voltage. Equation 5 is applied to each measurement point before applying the hotwire calibration. Calibration was done the same day as the velocity measurements, so the temperature difference was not too large, never exceeding 2.6°C (Hultmark and Smits [6] suggest a temperature correction that considers temperature dependent fluid properties for variations greater than 2-3 degrees).

Figures 26 and 27 show surveys of time average and root-mean-square fluctuations of velocity vertically above the model surface for all four circumferential positions. Two different types of traverses

were completed- the first was a 'short range' traverse which had a smaller step size (ranging from 0.2 mm – 0.5 mm, with smaller step sizes used close to the probe surface) and only went up to ~6 mm away from the probe surface. The 'long range' traverse had a larger step size (ranging from 2 mm – 19 mm) and extended nearly 160 mm away from the model surface. The short range traverse is meant to capture part of the boundary layer, which can be seen to be about 3mm thick. Note that the y position is vertical distance, not wall normal distance, and |U| is the magnitude of velocity since the hot film is sensitive to both streamwise, U_x, and vertical, U_y, components of velocity, i.e., $|U| = \sqrt{U_x^2 + U_y^2}$. High $|U|_{rms}$ values near the surface of the model indicates the boundary layer is turbulent. The model scale VMS and VASI probes were both outside of the boundary layer.

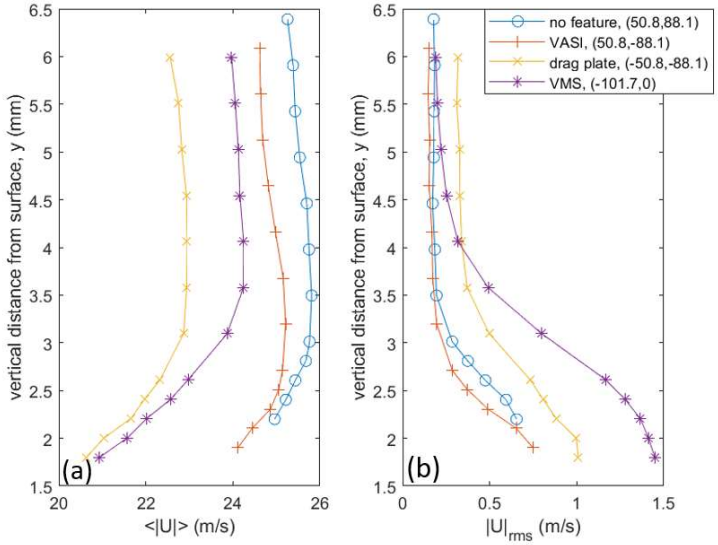


***Figure 26**: Survey of (a) mean velocity and, (b) root-mean-square of velocity fluctuation close to the model surface (short-range traverse) up to y ~ 6 mm at X,Y positions indicated in legend.*

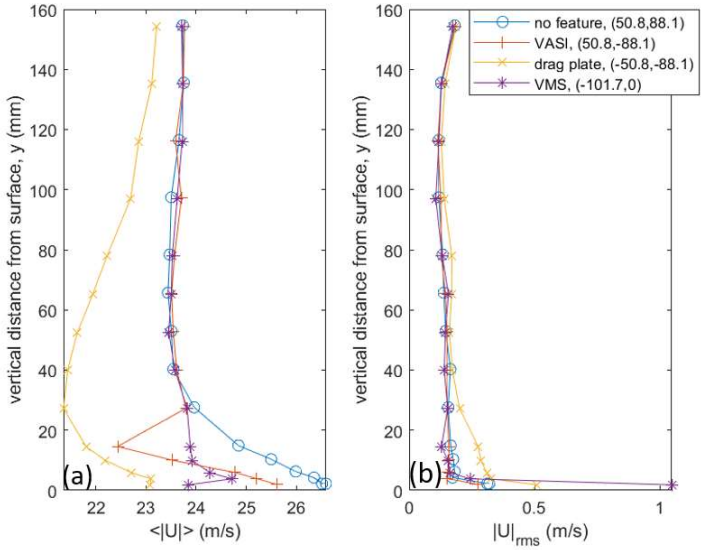


***Figure 27**: Survey of (a) mean velocity and, (b) root-mean-square of velocity fluctuation over a longer distance from the model surface (long-range traverse) up to y ~ 154 mm at X,Y positions indicated in legend.*

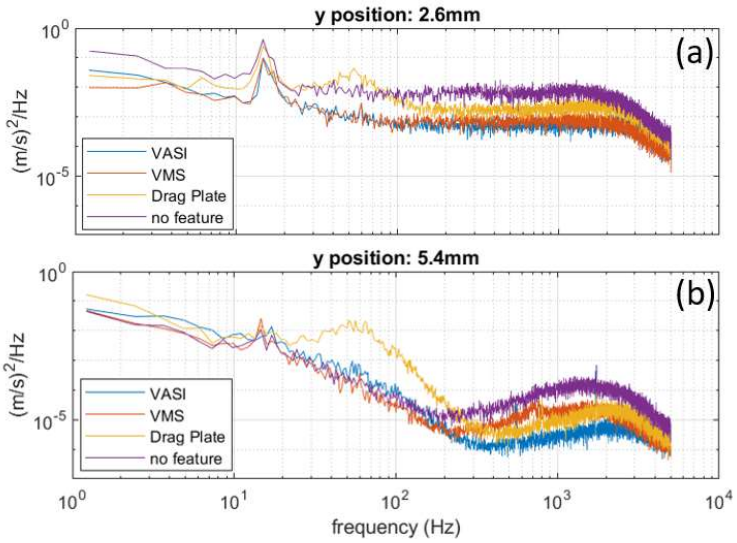


***Figure 28**: Power spectral density of velocity fluctuations at two vertical distances from surface, y (mm).*

The long range traverse measured the velocity variation farther away from the model surface and to check attainment of the free-stream value. For example, in Figure 26 the velocity profiles differ by 1-2 m/s at most points between the different cases. Figure 27 shows that this is due to the VASI, VMS, or drag plate decelerating the flow locally close to the surface of the model, while at ~25 mm and above, all velocity profiles are similar except for the drag plate, which understandably disturbs the flow much farther away from the model than the VMS and VASI probes. The VASI probe also decelerated the flow at a height of ~15 mm, which corresponds to the height of the forward extending part of that probe on the wind tunnel model. The other effect that is observed is the acceleration of the potential flow around the model. This results in the interesting shape of the velocity profiles in Figure 27 where the velocity increases as the hot film probe exits the boundary layer until it reaches about 26 m/s, then decreases towards the free stream velocity.

Though the hot film traverses were helpful to understand the flow structure around the wind tunnel model, it is difficult to extrapolate information such as the boundary layer thickness and the exact extent to which the potential flow around the model is accelerated due to the large difference in Reynolds number between the model and full-scale vehicle, the presence of a trip strip on the upstream side of the model, and the fact that the wind tunnel walls upstream of the model may impact the streamlines around the model. Despite these uncertainties, the hot film measurements were still an important check to verify the boundary layer was turbulent, and examine the frequency content of the velocity fluctuations in and outside the boundary layer.

Power spectral densities were calculated from the velocity measurements and are shown at two y positions in Figure 28. Two frequency peaks are evident. At a y position of 2.6 mm, which falls within the boundary layer, a sharp peak occurs around 15 Hz, a frequency that roughly corresponds to the peak frequency of the pressure fluctuations measured in this region of the model. Another broader peak is seen especially at the y position of 5.4mm centered at ~60 Hz for the spectrum measured in front of the drag plate. This frequency corresponds also to the pressure fluctuation peak frequency measured in front of the drag plate shown in Figure 19(c). The velocity fluctuation levels generally are higher at y=2.6mm vs 5.4mm, indicating a fully developed turbulent boundary layer over the model. The higher Reynolds number of the flow over the Zephyr probe during Venusian descent is also expected to produce a fully developed turbulent boundary layer. This correspondence of the boundary layer states increase confidence in the present test data.

4 Summary and conclusions

Despite a slow descent velocity, the Zephyr probe will be subjected to a high level of surface-pressure fluctuations due to the very high density of the Venus atmosphere. This motivated conducting a wind tunnel test using a 25% scaled model to establish the acoustics environment. The model was an SLA 3D printed model and incorporated eighteen ¼" condenser microphones as well as a variety of swappable inserts to compare different geometry configurations. Three rows of trip dots and a trip strip were added to the model to ensure a turbulent boundary layer in the wind tunnel test. The model was mounted on a sting and a strut. A McMaster Henderson airfoil shaped fairing was placed around the strut (vertical support) to minimize noise generation from the mounting fixture.

Testing was conducted in two wind tunnels in the NASA Ames Fluid Mechanics Lab. The Lifesaver tunnel at speeds ranging 13 m/s- 25 m/s and the Test Cell 2 wind tunnel at speeds ranging from 20 m/s to 49 m/s. Prior to mounting the model in the wind tunnels, background pressure fluctuations were measured using single microphones placed in the empty test sections. The background information was used to remove the background tones from the more heavily contaminated TC2 data. Microphone data was collected over these velocity ranges as well as yaw angles of -10 to +10 degrees, and for roll angles of 0, 45, and 90 degrees. Additionally, smoke-laser flow visualization and hot-film velocity surveys were conducted. The flow visualization showed a large, separated wake extending far behind the model, and a smaller, separated recirculation zone in front of the drag plates. The hot film survey showed a thin turbulent boundary layer under a fast moving potential flow over the probe.

Microphone data scaled to the flight-scale showed overall levels of 137 dB on the front of the probe, 144 dB on the rear of the probe, and an overall maximum directly in front of the drag plate of 157 dB. More generally, 3 primary spectral shapes were observed corresponding to three different flow regions on the model. Corcos model parameters are calculated for use as input into vibro-acoustic analysis software. The 2-point space-time correlations showed two distinct origins and Corcos parameters- an energetic hydrodynamic fluctuations propagating with speeds 0.4U-0.8U, and a weaker, high frequency fluctuations propagating at close to the speed of sound.

Lastly, eight different geometric configurations were tested. The size of the drag plates, different treatments at port openings in the aeroshell, different spin vane angles, and the effect of closing the front window port were studied, but none of the geometry changes were deemed to provide a significant benefit.

5 References

[1] J. B. Garvin, S. A. Getty, G. N. Arney, N. M. Johnson, E. Kohler, K. O. Schwer, M. Sekerak, A. Bartels, R. S. Saylor, V. E. Elliott and a. others, "Revealing the mysteries of Venus: The DAVINCI mission," *The Planetary Sciences Journal,* vol. 3, p. 117, 2022.

[2] W. K. Blake, Mechanics of Flow-Induced Sound and Vibrations, vol. II, San Diego, CA: Academic Press, 1986.

[3] P. G. Bremner and J. F. Wilby, "Aero-Vibro-Acoustics: Problem Statement and Methods for Simulation-Based Design Solution," in *8th AIAA/CEAS Aeroacoustics Conference& Exhibit*, Breckenridge, Colorado.

[4] P. T. Soderman and C. S. Allen, "Microphone Measurements in and Out of Airstream. In: Mueller, T.J. (eds) Aerosacoustic Measurements.," Springer, Berlin, Heidelberg, 2002.

[5] L. E. Kinsler, A. R. Frey, A. B. Coppens and J. V. Sanders, Fundamentals of Acoustics 4th Ed., New York, NY: Joh Wiley & Sons, Inc., 2000.

[6] M. Hultmark and A. J. Smits, "Temperature corrections for constant temperature and constant current hot-wire anemometers," *Measurement Science Technology,* no. 21, 2010.